ChemComm

Accepted Manuscript

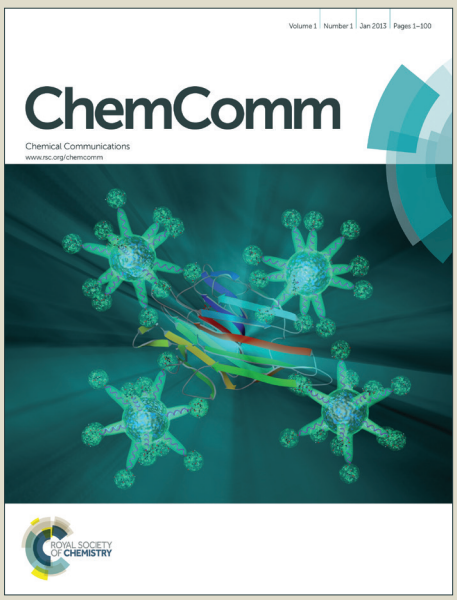

ROYAL SOCIETY OF CHEMISTRY

www.rsc.org/chemcomm

ChemComm

RSCPublishing

COMMUNICATION

A Dual Colorimetric-Ratiometric Fluorescent Probe NAP-3 for Selective Detection and Imaging of Endogenous Labile Iron (III) Pools in *C. elegans*

Cite this: DOI: 10.1039/xoxxoooooox

Atul Goel,*[a] Shahida Umar,[a] Pankaj Nag,[a] Ashutosh Sharma,[a] Lalit Kumar,[b] Shamsuzzama,[b] Zakir Hossain,[c] Jiaur R. Gayen,[c] Aamir Nazir[b]

Received ooth January 2012,
Accepted ooth January 2012

DOI: 10.1039/xoxxoooooox

www.rsc.org/

The discovery of an iron (III)-selective ratiometric fluorescent probe to detect and visualize endogenous labile iron pools in living organisms at molecular-level has been long awaited. Herein we report the first dual colorimetric and ratiometric fluorescent probe Naphtho[2,1-*b*][1,10]phenanthroline NAP-3 for selective and 'direct' visualization of labile iron (III) pools in a multicellular organism *Caenorhabditis elegans*.

Iron is an essential redox-active element in all living organisms controlling indispensable physiological and pathophysiological functions.[1] The bulk of the iron present in biological systems is tightly bound to various proteins.[2] Only a fraction of iron is free and exists as cytosolic labile iron pool (LIP) consisting of both the ionic forms (Fe^{2+} and Fe^{3+}) in dynamic equilibrium.[3] If the cellular homeostasis of labile iron gets disturbed, it can trigger uncontrolled Fenton reaction[4] leading to peroxidative tissue damage and thus causing various diseases, such as Alzheimer's disease (AD), Parkinson's disease (PD), and different types of cancers.[5] The complexity of redox chemistry of labile iron and its role in biological processes remain a challenge for chemists and biologists due to the dearth of iron-selective, sensitive and cell-permeable ratiometric fluorescent probes.[6] Although fluorogenic iron probes like calcein, fluorescein-deferoxamine (FL-DFO), Phen green SK and Phen green FL have been explored for cell imaging applications, they provide information through fluorescence quenching readouts, and exhibit poor selectivity between the two spin states of iron and nonspecific turn-off response with other interfering transition metal ions.[6,7] Few examples of Fe (II)[8] and Fe (III)[9] selective fluorescent sensors and chemodosimeters are reported in the literature with or without cell imaging studies. Remarkably, Tang et al. in 2011 reported the first ratiometric fluorescent probe for the selective detection of both exogenous and endogenous labile Fe (II) in live human liver HL7702 cells.[10] Recently, Guo et al in 2012 reported rhodamine based turn on fluorescent probe 'RPE' for imaging labile Fe (III) pools in live neuronal cells.[11] To the best of our knowledge, none has reported Fe (III)-selective ratiometric probe for in vivo visualization of LIP in a multicellular organism. From the perspective of accurate and quantitative analysis, ratiometric sensors and reporters have distinct advantage over single emission intensity-based probes because of their self-calibration/built-in environmental correction via two selected emission wavelengths.[12]

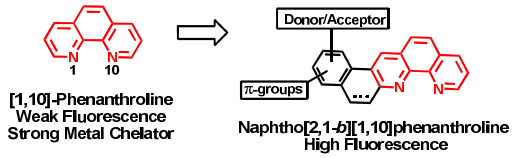

Fig. 1 Designing of Naphtho[2,1-*b*][1,10]phenanthrolines (NAPs).

Commercially available Phen green probes possess [1,10]-phenanthroline (PHT) scaffold, which is an entropically balanced iron-metal chelating ligand but exhibits weak fluorescence due to low lying π–π* and n–π* singlet excited states.[13] Though enormous efforts have been made in the past to improve its emission intensity by introducing π-conjugated systems mainly at the 2,9- 3,8- and 4,7-positions, researchers still rely on fluorescent tags. Henceforth PHT-based commercial iron probes Phen green SK/FL or siderophores (deferoxamine) are appended with fluorescein label, yet they suffer with nagging problems of quenching readouts and/or poor selectivity.[3,6] Addressing these issues and considering the necessity for selective ratiometric fluorescent probes for iron, we conceptually designed a novel[14] naphtho[2,1-*b*][1,10]-phenanthroline (NAP) framework (surprisingly yet unknown in the literature) equipped with well-conjugated donor-acceptor (D-A) and chromophoric π-groups to induce effective charge transfer during preferential binding of metal to the phenanthroline receptor (Fig. 1).

Our research group is engaged in target-based design and synthesis of new fluorescent dyes for their application in material[15] and biological sciences.[16] We have previously shown that controlled tuning of π-conjugation and appropriate positioning of D-A moieties dramatically modulate the optical properties of aromatic and heterocyclic compounds.[15] The synthetic methodology adopted for the synthesis of designed D-A NAPs is outlined in Scheme 1. The key intermediates 2*H*-pyran-2-ones **3a-d** were prepared from easily accessible precursor α-oxo-ketene-*S,S*-acetal (**1**) and substituted acetophenones (**2a-d**).[15] This was followed by the substitution of the methylsulfanyl group in

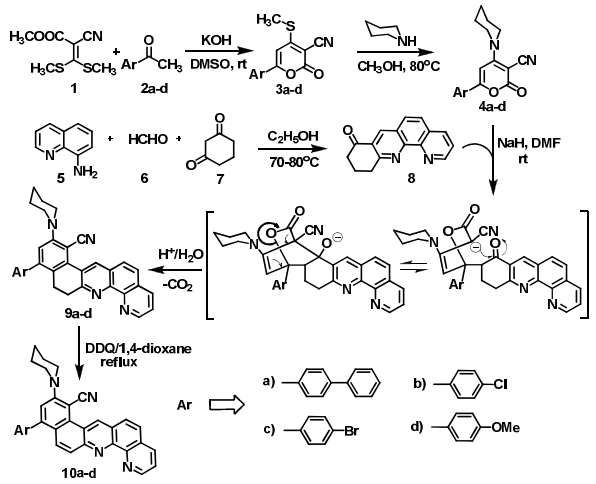

Scheme 1 Synthesis of Naphtho[2,1-*b*][1,10]phenanthrolines (NAPs).

3a-d by a piperidine donor group to furnish D-A appended 6-aryl-2-oxo-4-piperidin-1-yl-2*H*-pyran-3-carbonitriles (**4a-d**) in good yields.[15] The chelating precursor 10,11-dihydrobenzo[*b*][1,10]phenanthrolin-8(9*H*)-one (**8**) was prepared via three-component condensation of 8-aminoquinoline with formaldehyde and 1,3-cyclohexane-dione in good yield (Scheme 1). Further, Michael addition of the conjugate base of **8** to the lactones **4a-d** at position 6 followed by intramolecular cyclization afforded 11-aryl-9-(piperidin-1-yl)-12,13-dihydronaphtho[2,1-*b*][1,10]-phenanthroline-8-carbonitriles **9a-d**. To extend π-conjugation, the compounds **9a-d** were aromatized with DDQ in dioxane at reflux conditions to get the desired NAPs **10a-d**.

The absorption and emission characteristics of the designed NAPs **9a-d** and **10a-d** were investigated in aqueous medium (10^{-5} M, triple distilled water TDW/DMSO, 9:1, v/v) at pH 7.0-7.4 (Figs. S1 and S2, Table S1, ESI†). The iron-sensing studies of NAPs in the presence of perchlorate salts of Fe^{2+} and Fe^{3+} revealed that only Fe^{3+} exhibited a visible color change (colorimetric response, Fig. 2a, Figs. S3-S6, ESI†) and a ratiometric fluorescence response in **10a-d** (Figs. S3-S5, ESI†) with **10c** (**NAP-3**) being the best having a well-defined isoemission point at 590 nm (Fig. 2b, Fig S7, ESI†). The aqueous solution of **NAP-3** exhibited an absorption maximum at 300 nm (π-π* transition) with a low intensity band at 368 nm (n-π* transition), and a green-yellow fluorescence band with a maximum at 544 nm (Fig. 2). Upon addition of increasing concentrations of Fe^{3+} ions, we observed emergence of a new peak with maximum at 580 nm in the absorption spectrum changing the solution color from light yellow to reddish pink thereby

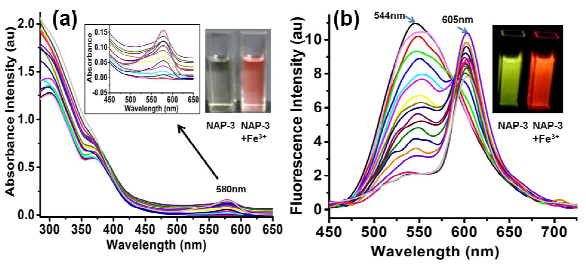

Fig. 2 (a) Absorption and (b) Ratiometric fluorescence spectra of **10c** (**NAP-3**) after 1 h upon addition of increasing concentrations of Fe^{3+} (0–6.8 × 10^{-4} M). [**NAP-3**] = 2.5 × 10^{-5} M, λ_{ex}= 365 nm. During the titration studies, pH of the solutions were maintained to 7.0-7.4 using 0.01M NaOH solution.

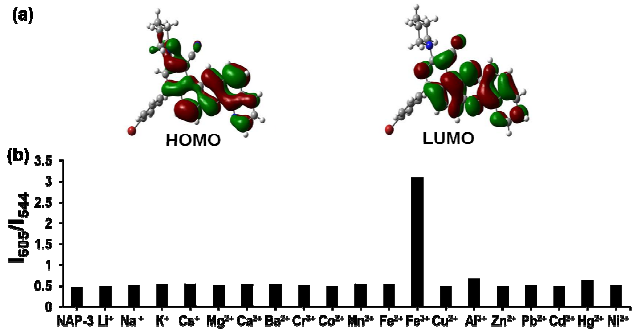

Fig. 3 (a) Computed molecular orbital energy diagrams of **NAP-3** as obtained from TDDFT calculations. (b) Selectivity studies of **NAP-3** (2.5 × 10^{-5} M) in the absence or presence of a series of metal ions (5 × 10^{-4} M) after 1 h upon addition of metal ion at λ_{ex}= 365 nm.

offering **NAP-3** as a Fe^{3+}-selective 'naked-eye' chemosensor. Correspondingly in the emission spectrum, the peak at 544 nm decreased and a new peak appeared at 605 nm with the increasing concentration of Fe^{3+}. The ratiometric response of fluorescence intensities (I_{605}/I_{544}) enhanced from 0.48 to 4.1 with a final enhancement factor over 8.5 fold (Fig. S8, ESI†). The titration studies with **NAP-3** revealed a good linearity between the fluorescence intensity ratio and Fe^{3+} concentration with a detection limit of approximately 9.1×10^{-9} M (Fig. S9, ESI†) that allowed the quantification of Fe^{3+} by a ratiometric fluorescence method[17]. Further Job's plot[18] established a 2:1 binding stoichiometry of **NAP-3** with Fe^{3+} (Fig. S10, ESI†), which was supported by mass spectrometry (Fig. S11, ESI†). The binding constant for **NAP-3** was determined as 9.36 × 10^{10} M^{-2} by non-linear regression analysis[19] (Fig. S12, ESI†). The fluorescence property of the probe **NAP-3** at different pHs (1.8–10.7) revealed no change in fluorescence intensity within pH 5.5–8.3 but a gradual decrease in the intensity was observed beyond this range (Fig S13, ESI†).

It is interesting to note that donor-acceptor functionalized naphtho[2,1-*b*][1,10]-phenanthroline **NAP-3** selectively binds to Fe^{3+} but not to Fe^{2+} (Figs. S6-S7, ESI†). This is contrary to the nature of 1,10-phenanthroline, which selectively binds to Fe^{2+} (Figs. S14-S15, ESI†). To understand the electronic behaviour of **NAP-3**, the geometries were optimized at DFT/B3LYP level using a 6-31G(d,p) basis set and time-dependent density functional theory (TDDFT) calculations were performed using a B3LYP/6-311++G(d,p) method.[20] The energies of the HOMO and LUMO levels, HOMO-LUMO gap, main orbital transition, and oscillator strength *f* are listed in Table S2 (ESI†). Fig. 3a shows the theoretically computed molecular orbitals in the ground states for the probe **NAP-3**. TDDFT results revealed two prominent electronic transitions observed at 305 nm (HOMO-2 to LUMO+1) and 383 nm (HOMO to LUMO). The electron density of the HOMO is delocalized over the piperidine donor moiety and the neighbouring naphthophenanthroline ring, while the LUMO is delocalized on the naphthophenanthroline moiety and the nitrile acceptor group (Fig. 3a). The electronic transition at higher wavelength (HOMO to LUMO) corresponds to an intramolecular charge-transfer (ICT) band. The presence of conjugated donor-acceptor moieties enhanced the charge density over phenanthroline ring of **NAP-3** facilitating the formation of ligand to metal charge transfer (LMCT) complex with Fe^{3+}. In contrast, 1,10-phenanthroline forms metal to ligand charge transfer (MLCT) complex with Fe^{2+}.[21]

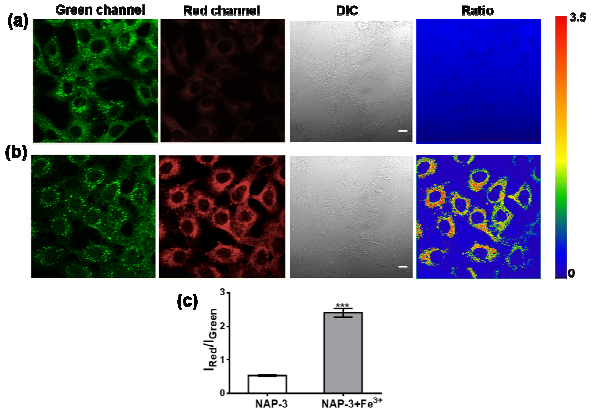

Fig. 4 (a) HepG2 cells incubated with **NAP-3** (3 μM, 24 h). (b) HepG2 cells incubated with **NAP-3** after ferric citrate (5×10^{-4} M, 24 h) supplementation. (c) Ratiometric quantification of relative fluorescence intensity of confocal microscopy images by image J software, ***p < 0.001. Green channel: λ_{ex} = 405 nm, λ_{em} = 505–550 nm. Red channel: λ_{ex} = 561 nm, λ_{em} = 575 nm long pass. Error bars are ± s.e.m. (n = 3). Scale bar: 10 μm.

The selectivity studies of **NAP-3** in the presence of high concentration (20 equiv.) of perchlorate salts of Li^+, Na^+, K^+, Cs^+, Mg^{2+}, Ca^{2+}, Ba^{2+}, Cr^{3+}, Co^{2+}, Mn^{2+}, Fe^{2+}, Fe^{3+}, Cu^{2+}, Al^{3+}, Zn^{2+}, Pb^{2+}, Cd^{2+}, Hg^{2+}, Ni^{2+} revealed that only Fe^{3+} triggered a dramatic increase in the emission ratio I_{605}/I_{544}, while other metal ions were either silent or induced minor ratiometric response (Fig. 3b, Fig. S17, ESI†). In order to confirm the selectivity of **NAP-3** for Fe^{3+} over Fe^{2+}, we conducted experiments under reducing (Fe^{3+} and hydroxylamine) and oxidizing (Fe^{2+} and hydrogen peroxide) environments (Figs. S18 and S19, ESI†). To our delight, **NAP-3** successfully discriminated Fe^{3+} over Fe^{2+}. We further conducted competitive experiments of **NAP-3** with a known strong Fe^{3+} chelator deferoxamine (DFO). We observed that in the presence of DFO, **NAP-3** could not bind to Fe^{3+}; while in the presence of **NAP-3**, DFO failed to remove Fe^{3+} from the complex (NAP-3.Fe^{3+}) possibly due to steric hindrance (Fig. S20, ESI†).

Promising selectivity of **NAP-3** for Fe^{3+} in both reducing and oxidizing environments and aqueous compatibility encouraged us to detect and visualize labile Fe^{3+} in living systems. Since small molecules like cysteine and glutathione present in cellular environment may interact with the probe, we examined the fluorescence response of **NAP-3** in the presence of these molecules (Fig. S21, ESI†). Gratifyingly, no change in the fluorescence spectra of **NAP-3** probe was observed. Thereafter confocal fluorescence imaging experiments were carried out with HepG2 cells considering liver as a major iron storage organ of the body.[8] We observed that treatment of cells with different concentrations (nanomolar to micromolar) of **NAP-3** exhibited a concentration-dependent staining pattern with 3 μM showing the best results (Fig. 4a, S22, ESI†). The cells incubated with **NAP-3** (3 μM) for 24 h exhibited intense intracellular fluorescence in the green channel (505–550 nm) but no fluorescence in the red channel (Long pass 575 nm) was observed (Fig. 4a). However, HepG2 cells pretreated with ferric citrate (5×10^{-4} M, 24 h) followed by incubation with **NAP-3** (3 μM, 24 h) showed significant increase in intracellular fluorescence in the red channel due to the formation of the complex of **NAP-3** in situ with exogenously supplemented Fe^{3+} (Fig. 4b). Furthermore, **NAP-3** exhibited significant intracellular ratiometric fluorescence response (Fig. 4c). **NAP-3** showed no cytotoxicity under the conditions used for cell imaging (Fig. S23, ESI†). Therefore, the *in vitro* cell studies demonstrated that **NAP-3** is a cell-permeable fluorescent probe to detect elevated levels of Fe^{3+} via exogenous supplementation and may be used for in vivo imaging of labile iron.

The soil nematode *Caenorhabditis elegans* is a model of choice for studying regulatory mechanisms associated with iron metabolism due to homology with human gene sequences.[22] Electron paramagnetic resonance (EPR) spectroscopy has been used as a tool to 'indirectly' measure free Fe^{3+} levels *in vivo* in *C. elegans*.[23] In an attempt to visualize LIP 'directly' in an organism, we examined *in vivo* iron binding specificity of **NAP-3** in wild type (N2) *C. elegans* by confocal fluorescence imaging experiments. We observed that treatment of worms with 3 μM of **NAP-3** for 24 h exhibited staining in the green channel, while staining was weak in the red channel (Fig. 5a, see zoomed images). The staining in the red channel implicated that **NAP-3** has access to Fe^{3+} present in LIP of wild type *C. elegans*. In order to confirm that the fluorescence in the red channel is due to the formation of Fe^{3+} complex and not by **NAP-3** alone, we measured the fluorescence of **NAP-3** at 561 nm excitation and no fluorescence in red channel was observed (Fig. S25, ESI†). These results implicated the detection of Fe^{3+} present in the LIP by the probe **NAP-3**.

On exogenous Fe^{3+} supplementation, there was no increase in the fluorescence intensity in the red channel as compared with only **NAP-3** treated groups (data not shown). These results indicated that to maintain iron homeostasis, worms might have triggered iron regulatory mechanisms associated with ferritins (FTN-1 and FTN-2), which are transcriptionally regulated by iron.[24] Thereby we repeated the experiments with *ftn-1* silenced *C. elegans* (RNAi induced silencing of gene). Interestingly at this time we observed significantly enhanced signals in the red channel (Fig. 5b) as compared to wild type strain (Fig. 5a). These results supported the previous findings[25] suggesting that reduced level of ferritins causes elevation of free iron content in the cytosol. Furthermore, the ratio of the intensities (I_{Red}/I_{Green}) was increased by 3 fold ($p < 0.001$) (Fig. 5c). The confocal imaging results showed a marked staining pattern in the worm body, posterior to pharyngeal region particularly concentrated around the gut region. It has been reported that *ftn-1* is up-regulated in the presence of exogenous iron supplementation, and down-regulated on treatment with an iron chelator.[26] Therefore to cross-examine whether **NAP-3** detected Fe^{3+} present in endogenous iron pool, we carried out quantitative real time PCR (qPCR) assays to quantify the levels of *ftn-1* mRNA in worms. We observed 2.8 fold ($p < 0.01$) down-regulation and 3.7 fold ($p < 0.01$) up-regulation of *ftn-1* mRNA levels in worms from **NAP-3** treated and Fe^{3+}-treated groups respectively (Fig. 5d). Upon treatment with both **NAP-3** and Fe^{3+}, a 1.5 fold reduction ($p < 0.05$) in levels of *ftn-1* mRNA was observed as compared to iron-treated group (Fig. 5d). These results unambiguously confirmed that ratiometric probe **NAP-3** is capable of detecting labile iron pool in *C. elegans*. This is the first report to visualize LIP in an organism with remarkably high selectivity and in analytically advantageous ratiometric manner.

In summary, we have designed and synthesized a novel Fe^{3+} selective dual colorimetric and ratiometric fluorescent probe **NAP-3** for detection and visualization of exogenous Fe^{3+} in *in vitro* (HepG2 cell line) and for the first time in *in vivo* (Wild type and *ftn-1* silenced *C. elegans*) models. The potential of **NAP-3** for binding to labile iron pool in wild type *C. elegans* was further established by monitoring the

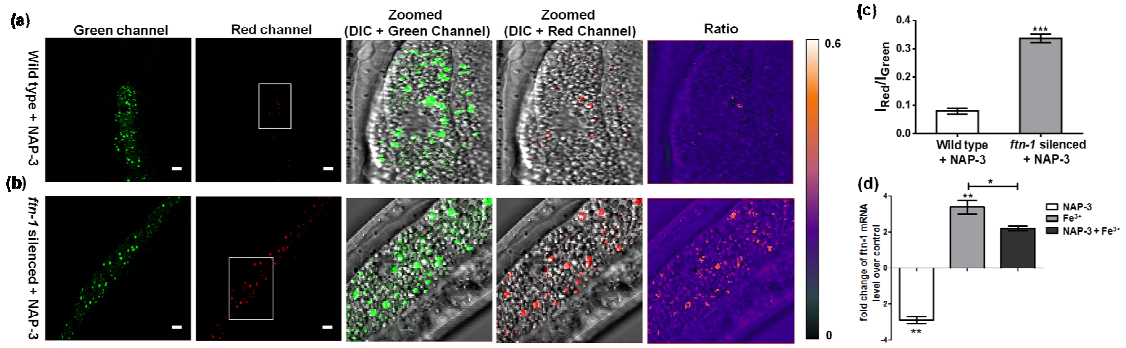

Fig. 5 (a) Wild type (N2) *C. elegans* treated with 3 μM **NAP-3** (3 μM, 24 h). (b) *ftn-1* silenced *C. elegans* treated with 3 μM **NAP-3**. (c) Ratiometric quantification of relative fluorescence intensity of confocal microscopy images by image J software, ***p < 0.001. (d) Quantitative Real Time PCR analysis of *ftn-1* gene (fold change) in various groups using wild type strain of *C. elegans*. *p < 0.05, **p < 0.01 (with respect to OP50 treated control). Green channel: λ_{ex} = 405 nm, λ_{em} = 505–550 nm. Red channel: λ_{ex} = 561 nm, λ_{em} = 575 nm long pass. Each experiment was repeated three independent times. Error bars are ± s.e.m. (n = 3). Scale bar: 10 μm.

mRNA levels of iron responsive gene *ftn-1 via* qPCR analysis. The high selectivity of **NAP-3** towards Fe^{3+} and its biocompatibility open new avenues to unravel the mysteries of the cellular dynamics of iron homeostasis and the role of labile iron pools associated with oxidative stress produced during Fenton chemistry. Further studies in these directions are underway.

The work is supported by the Council of Scientific and Industrial Research, New Delhi (BSC0102 and BSC0114). Authors thank K. Mitra and K. Singh for confocal fluorescence imaging of the samples. The CDRI communication number is 8873.

Notes and References

[a]*Medicinal and Process Chemistry Division,* [b]*Department of Toxicology* [c]*Department of Pharmacokinetics and Metabolism, CSIR-Central Drug Research Institute, Lucknow 226031, India; fax: +91-522-2771941; Tel.: +91-522-2772450; e-mail: atul_goel@cdri.res.in*

*†Electronic Supplementary Information (ESI) available: [Spectroscopic Characterization data, ^{1}H, ^{13}C NMR spectra and absorption, and fluorescence spectra of all the compounds **9a-d** and **10a-d**. Cytotoxicity data, materials and methods]. See DOI: 10.1039/b000000x/*

1. M. W. Hentze, M. U. Muckenthaler and N. C. Andrews, *Cell*, 2004, **117**, 285.
2. P. A. Frey and G. H. Reed, *ACS Chem. Biol.*, 2012, **7**, 1477.
3. W. Breuer, M. Shvartsman, and Z. I. Cabantchik, *Int J Biochem Cell Biol.*, 2008, **40**, 350.
4. H. J. H. Fenton, *J. Chem. Soc. Trans*, 1894, **65**, 899.
5. (a) S. J. Dixon and B. R. Stockwell, *Nat. Chem. Biol.*, 2014, **10**, 9; (b) D. B. Kell, *BMC Medical Genomics,* 2009, **2**, 1.
6. D. W. Domaille, E. L. Que and C. J. Chang, *Nat. Chem. Biol.*, 2008, **4**, 168.
7. (a) S. Epsztejn, O. Kakhlon, H. Glickstein, W. Breuer and Z. I. Cabantchik, *Anal. Biochem.,* 1997, **248**, 31; (b) F. Petrat, U. Rauen and H. D. Groot, *Hepatology*, 1999, **29**, 1171.
8. (a) T. Hirayama, K. Okuda and H. Nagasawa, *Chem. Sci.*, 2013, **4**, 125; (b) H. Y. Au-Yeung, J. Chan, T. Chantarojsiri and C. J. Chang, *J. Am. Chem. Soc.*, 2013, **135**, 15165.
9. (a) S. K. Sahoo, D. Sharma, R. K. Bera, G. Crisponi and J. F. Callan, *Chem. Soc. Rev.*, 2012, **41**, 7195; (b) S. Sen, S. Sarkar, B. Chattopadhyay, A. Moirangthem, A. Basu, K. Dharad and P. Chattopadhyay, *Analyst*, 2012, **137**, 3335; (c) R. Wang, F. Yu, P. Liu and L. Chen, *Chem. Commun.*, 2012, **48**, 5310; (d) S. Goswami, S. Das, K. Aich, D. Sarkar, T. K. Mondal, C. K. Quah and H.K. Fun, *Dalton Trans.,* 2013, **42**, 15113; (e) S. Goswami, K. Aich, S. Das, A. K. Das, D. Sarkar, S. Panja, T. K. Mondal and S. Mukhopadhyay, *Chem. Commun*., 2013, **49**, 10739.
10. P. Li, L. Fang, H. Zhou, W. Zhang, X. Wang, Na Li, H. Zhong, and B. Tang, *Chem. Eur. J.,* 2011, **17**, 10520.
11. Y. Wei, Z. Aydin, Y. Zhang, Z. Liu and M. Guo, *ChemBioChem*, 2012, **13**, 1569.
12. (a) E. A. Lemke and C. Schultz, *Nat. Chem. Biol.*, 2011, **7**, 480; (b) S. Maruyama, K. Kikuchi, T. Hirano, Y. Urano and T. Nagano, *J. Am. Chem. Soc.*, 2002, **124**, 10650.
13. G. Accorsi, A. Listorti, K. Yoosaf and N. Armaroli, *Chem. Soc. Rev.*, 2009, **38**, 1690.
14. A. Goel, S. Umar, P. Nag, A. Nazir, L. Kumar, Shamsuzzama, J. R. Gayen, and Z. Hossain, Substituted Naphtho[2,1-*b*][1,10]-phenanthroline-based fluorescent dyes and application thereof. CSIR Patent application No. 1942/DEL/2014 (India, 2014).
15. (a) A. Goel, A. Sharma, M. Rawat, R. S. Anand, and R. Kant *J. Org. Chem.* 2014, 79, 10873; (b) A. Goel, V. Kumar, S. P. Singh, A. Sharma, S. Prakash, C. Singh and R. S. Anand, *J. Mater. Chem.*, 2012, **22**, 14880; (c) A. Goel, S. Chaurasia, M. Dixit, V. Kumar, S. Prakash, B. Jena, J. K. Verma, M. Jain, R. S. Anand and S. S. Manoharan, *Org. Lett.*, 2009, **11**, 1289.
16. A. Goel, A. Sharma, M. Kathuria, A. Bhattacharjee, A. Verma, P. R. Mishra, A. Nazir and K. Mitra, *Org. Lett.*, 2014, **16**, 756.
17. B. Zhu, C. Gao, Y. Zhao, C. Liu, Y. Li, Q. Wei, Z. Ma, B. Du and X. Zhang, *Chem. Commun.*, 2011, **47**, 8656.
18. H. Zheng, X.-J. Zhang, X. Cai, Q.-N. Bian, M. Yan, G.-H. Wu, X.-W. Lai and Y.-B. Jiang, *Org. Lett.*, 2012, **14**, 1986.
19. L. N. Neupane, J.-Y. Park, J. H. Park and K.-H. Lee, *Org. Lett.*, 2013, **15**, 254.
20. (a) G. J. Zhao and K. L. Han, *Acc. Chem. Res.,* 2012, **45,** 404; (b) G.Y. Li, G. J. Zhao, Y.H. Liu, K. L. Han and G. Z. He, *J. Comput. Chem.,* 2010, **31**, 1759; (c) G. J. Zhao, J. Y. Liu, L. C. Zhou and K. L. Han, *J. Phys. Chem. B,* 2007, **111**, 8940.
21. (a) M. Arifuzzaman, T. A. Siddiquee, M. R. Karim, A. H. Mirza and M. A. Ali, *Cryst Struct Theory Applicat.*, 2013, **2**, 159; (b) J. Burgess, S. Radulović, F. Sánchez, *Transition Met Chem*., 1987,**12**, 529; (c) R. Mayilmurugan, M. Sankaralingam, E. Suresh and M. Palaniandavar, *Dalton Trans.*, 2010, **39**, 9611; (d) M. Balamurugan, P. Vadivelub and M. Palaniandavar, *Dalton Trans.*, 2014, **43**, 14653.
22. C. P. Anderson and E. A. Leibold, *Front. Pharmacol.,* 2014, **5**, 1.
23. K. T. Pate, N. A. Rangel, B. Fraser, M. H. S. Clement and C. Srinivasan, *Anal. Biochem.,* 2006, **358**, 199.
24. S. J. Romney, C. Thacker and E. A. Leibold, *J. Biol. Chem.*, 2008, **283**, 716.
25. Y.-I. Kim, J. H. Cho, O. J. Yoo and J. Ahnn, *J. Mol. Biol.*, 2004, **342**, 421.
26. S. Valentini, F. Cabreiro, D. Ackerman, M. M. Alam, M. B. A. Kunze, C. W. M. Kay and D. Gems, *Mech. Ageing Dev.*, 2012, **133**, 282.